



ACADÉMIE
DES SCIENCES
INSTITUT DE FRANCE

Comptes Rendus

Géoscience

Sciences de la Planète

Chrystèle Sanloup, Clémence Leroy, Benjamin Cochain, Tobias Grützner,
Qi Chen, Yoshio Kono and Guoyin Shen


Iodine speciation in basaltic melts at depth

Published online: 12 December 2024

Part of Special Issue: Magma degassing and its impact on the Earth's atmosphere:
from magma oceans to lava lakes

Guest editors: Manuel Moreira (Institut des Sciences de la Terre d'Orléans Université
d'Orléans-CNRS-BRGM 1a rue de la Férollerie 45071 Orléans France), Bruno Scaillet
(Institut des Sciences de la Terre d'Orléans Université d'Orléans-CNRS-BRGM 1a rue
de la Férollerie 45071 Orléans France) and Clive Oppenheimer (Department of
Geography, University of Cambridge, Downing Place, Cambridge CB2 3EN, UK)

<https://doi.org/10.5802/crgeos.279>

 This article is licensed under the
CREATIVE COMMONS ATTRIBUTION 4.0 INTERNATIONAL LICENSE.
<http://creativecommons.org/licenses/by/4.0/>



*The Comptes Rendus. Géoscience — Sciences de la Planète are a member of the
Mersenne Center for open scientific publishing*

www.centre-mersenne.org — e-ISSN : 1778-7025



Research article

Magma degassing and its impact on the Earth's atmosphere: from magma oceans to lava lakes

Iodine speciation in basaltic melts at depth

Chrystèle Sanloup^{*,a,b}, Clémence Leroy^a, Benjamin Cochain^c, Tobias Grützner^d, Qi Chen^e, Yoshio Kono^f and Guoyin Shen^g

^a Institut de minéralogie, physique des matériaux et cosmochimie, Sorbonne Université, CNRS, 4 Place Jussieu, France

^b Institut Universitaire de France (IUF), Paris, France

^c Institut de minéralogie, physique des matériaux et cosmochimie, Sorbonne Université, CNRS, 4 Place Jussieu, Paris, France

^d Institut für Geowissenschaften, Goethe-Universität Frankfurt, Germany

^e Department of Earth Science & Environmental Change, University of Illinois at Urbana Champaign, Urbana, IL, USA

^f Department of Physics and Astronomy, Kwansei Gakuin University, Sanda, Japan

^g HPCAT, X-ray Science Division, Argonne National Laboratory, Argonne, USA

E-mails: chrystele.sanloup@sorbonne-universite.fr (C. Sanloup), cl.clemenceleroy@gmail.com (C. Leroy), benjamin.cochain@gmail.com (B. Cochain), tobias.gruetzner@outlook.com (T. Grützner), qichen22@illinois.edu (Q. Chen), yoshiokono@kwansei.ac.jp (Y. Kono), gyshen@anl.gov (G. Shen)

Abstract. The speciation of iodine in basalts has been investigated by combining in situ X-ray diffraction at high pressures and temperatures up to 4.9 GPa and 1600 °C, and Raman spectroscopy on recovered high pressure glasses at ambient conditions. Both methods point to iodine being oxidized in basalts, whether molten or quenched as glasses. Observed interatomic distances and Raman vibrational modes are consistent with iodine being dissolved as complex iodate groups alike polyiodates or periodates, not as IO₃⁻ groups. Iodine speciation in basalts therefore seems to reflect a trend amongst halogens, with lighter chlorine bonding to network modifying cations, and bromine changing affinity from network modifying cations to oxygen anions under pressure. In the absence of a fluid aqueous phase, iodine could thus reach the Earth's surface in basaltic magmas as an oxide, not as a reduced species.

Keywords. Iodine, Basalt, High pressure.

Funding. European Research council under the European Community's Seventh Framework Programme (FP7/20072013 Grant Agreement No. 259649), ANR Projet de Recherche Collaborative VOLC-HAL-CLIM (Volcanic Halogens: from Deep Earth to Atmospheric Impacts, ANR-18-CE01-0018), EU Marie Skłodowska-Curie Fellowship "ExCliso" (Project ID 101017762), CSC scholarship (#201806340094), DOE Office of Science by Argonne National Laboratory under Contract No. DE-AC0206CH11357.

Manuscript received 25 July 2024, revised 23 October 2024, accepted 4 November 2024.

*Corresponding author

1. Introduction

Halogens can provide key insights into magmatic processes ranging from partial melting to volcanic eruptions [Webster *et al.*, 2018] if their behaviour is fully understood from fluorine to iodine. However, iodine is the least investigated halogen in magmatic and volcanic processes, in relation with its lowest abundance both in magmas [Kendrick *et al.*, 2012, 2014] and in volcanic plumes [Aiuppa *et al.*, 2005]. It is nonetheless an important element as it impacts atmospheric chemistry through ozone depletion [Solomon *et al.*, 1994], having the largest ozone-depleting efficiency [Cuevas *et al.*, 2022].

As for most elements, iodine speciation controls its solubility, transport, and eventual elemental and isotopic fractionation between coexisting phases. Progresses have been made towards the understanding of its transfer between reservoirs, especially between magmas and aqueous fluids to assess the extent of its degassing [Bureau *et al.*, 2000, Leroy *et al.*, 2019], but not on its speciation in natural magmas. There are besides no available *in situ* data on iodine speciation in silicate melts, *i.e.* under high temperature (T) and high pressure (P) conditions. Available data on iodine speciation in silicate glasses have been obtained using Raman, X-ray photoelectron and/or X-ray absorption spectroscopies on borosilicate melts quenched from high P – T conditions [Ciccconi *et al.*, 2019, Morizet *et al.*, 2021], in order to understand and better predict iodine behaviour and eventual mobility in nuclear waste glasses. Consequently, there is a lack of data on iodine speciation in natural magmas in general, and in particular at the high P – T conditions at which they form and ascend.

Here, we report *in situ* high P – T synchrotron X-ray diffraction data (XRD) on basaltic magmas, and Raman spectroscopy data on recovered quenched glasses. High P are necessary to dissolve sufficient amount of iodine so that its effect on magmas properties can be measured, but more importantly because arc magmas that are produced at greater depths hence greater pressures than oceanic ridge basalts are the most relevant to investigate iodine speciation, due to recycling of marine sedimentary components that bring iodine to the arc magma source [Muramatsu and Wedepohl, 1998].

The choice of Saint Vincent island (Lesser Antilles arc) basalt [Pichavant *et al.*, 2002] and of Mount Etna

basalt (from 2002/2003 South scoria [Gennaro *et al.*, 2019]) was guided by the need to reflect a range of volatile-rich basalts, with high MgO Saint Vincent basalt being representative of one type of primary magma in subduction zones, and Mount Etna alkali basalt representative of later stage basalt differentiated through fractional crystallization and degassing.

2. Materials and methods

2.1. Glass synthesis

Starting natural basalt samples were ground, doped with NaI as iodine source, and with deionised milli-Q water added in the case of Saint Vincent basalt. When investigating the local environment of a trace element in a magma, one must reach a compromise between lowest amount possible and detection above noise level to avoid interaction between iodine ions that would occur for elevated concentrations. Two iodine levels were targeted, circa 3 wt% for the Saint Vincent basalt, and circa 1 wt% for the Etna basalt. Since iodine solubility increases with P , I-doping was done at 3.5 GPa and 1600 °C for the Saint Vincent basalt using platinum capsules welded at both ends, and at 1 GPa and 1350 °C for the Etna composition using gold–palladium capsules which have a lower T -stability but prevent Fe loss to the capsule unlike for Saint Vincent basalt that became almost FeO-free. Having two different FeO content turned out to be essential in assessing iodine local environment in the melt (*cf.* Section 3.2). For both compositions, I-free glasses were synthesized under the same conditions. High P – T conditions were generated by a Depth of the Earth piston cylinder press using a half inch talc-pyrex cell assembly with a graphite heater; T was monitored using a W/Re thermocouple, run duration at high T was one hour.

2.2. High P – T X-ray diffraction experiments

The recovered glass from piston cylinder press experiments was extracted from the platinum or gold–palladium capsule, crushed, and loaded in either graphite capsule (Saint Vincent basalt) or in single crystal diamond capsules with inner graphite caps and sealed under P by Pt–5%Rh caps (Etna basalt). High P – T conditions (Table 1) were achieved using a Paris-Edinburgh press with cell-assembly (Figure 1) as described in Yamada *et al.* [2011]. This

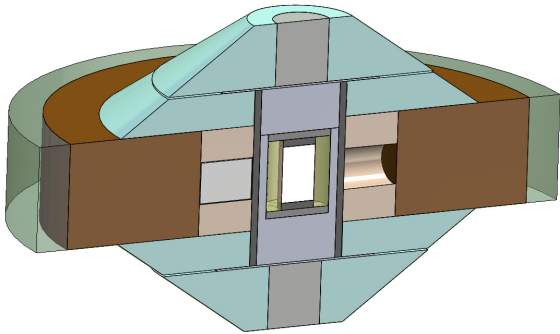


Figure 1. Sketch of the cell-assembly used for in situ high P - T X-ray diffraction experiments [Yamada *et al.*, 2011]. Sample (inner white rectangle) is packed either in a graphite capsule or in a single crystal diamond cylinder (as drawn here, inner diameter: 1.0 mm), covered by inner graphite caps and sealed by Pt-Rh caps.

cell-assembly is designed to optimize the sample signal by using low absorbing materials along the X-ray path (boron epoxy and hBN windows inside the MgO ring outside the graphite heater), while ZrO₂ parts away from the X-ray path insure cell-assembly stability at high P - T conditions. Talc powder was added on top and bottom of graphite capsules, to act as fO_2 buffer. Temperature was calculated from power- T curve calibrated against melting temperatures of salts [Kono *et al.*, 2014], and P was calculated from the cell volume of MgO cylinder surrounding sample capsule [Kono *et al.*, 2010]. Uncertainties on P and T are respectively 0.3 GPa and 80 °C. While most runs were carried at T above the liquidus, two experiments were run between solidus and liquidus T (TGH25 and TGH26).

In situ high P - T experiments were conducted using energy-dispersive XRD on beamline 16-BM-B at the Advanced Photon Source (Argonne, USA). The incident beam was collimated by tungsten slits (0.3 mm vertical \times 0.1 mm horizontal) and the diffracted signal was collected by an energy-dispersive germanium solid-state detector. In the molten state, X-ray diffraction data were collected at different 2θ angles (2°, 2.7°, 3.5°, 5°, 7°, 10°, 15°, 20°, and 27°) thus covering up to 15 Å⁻¹ in q -space ($q = 4\pi E \sin\theta / 12.398$, where E is the energy of the X-rays in keV ranging up to 125 keV).

The multi-angle energy dispersive X-ray diffraction spectra were converted into the structure factor $S(q)$ using analysis software package (aEDXD) program developed by Changyong Park [Kono *et al.*, 2014]. The real-space radial distribution function, $g(r)$, that described the short-order range structure (i.e. interatomic relations within 5–6 Å) was obtained by Fourier Transform of the spline smoothed $S(q)$:

$$g(r) = 1 + \frac{1}{4\pi r n} \int_0^{q_{\max}} q(S(q) - S_{\infty}) \sin(qr) dq \quad (1)$$

where n is the atomic density in atoms per Å³ ($n = N_A M / \rho$, with N_A the Avogadro's constant, M the mean atomic molar mass of samples, and ρ their mass density).

2.3. Starting and recovered samples analyses

Samples were polished for textural analyses using a Zeiss Ultra 55 field emission scanning electron microscope (SEM) at OSU Ecce Terra, Sorbonne Université, followed by chemical analyses (Table 1) carried at the Camparis center, Sorbonne Université, using a Cameca SX-FIVE electron probe microanalyser (EPMA) with accelerating voltage set at 15 keV, beam current at 4 nA, and a defocussed beam (7 μm radius).

Raman spectra were recorded on a Jobin Yvon Horiba HR460 spectrometer using a single-grating monochromator with 1500 gratings/mm and an argon laser (514.5 nm wavelength).

3. Results

3.1. Quenched texture and composition of starting and recovered glasses

Nanosize iodine droplets are observed on Saint Vincent basalt starting glasses (PC82 and PC83, Figure 2a), and could either be quench products or due to iodine oversaturation as those samples have the highest iodine content (Table 1). Such nanodroplets are not observed in other samples, including Saint Vincent glass recovered from XRD experiment which moreover was conducted at higher P (APS run 13) than during piston-cylinder press synthesis, i.e. at conditions of higher iodine solubility. Iodine was thus fully dissolved in molten basalts probed by XRD.

Recovered Etna basalt samples from XRD experiments, either I-doped or not, contain droplets of

Table 1. Chemical analyses (wt%). Starting and recovered samples

Sample <i>P-T</i> conditions	SiO ₂	TiO ₂	Al ₂ O ₃	FeO	MgO	CaO	Na ₂ O	K ₂ O	I	Total*
	(Standard deviations)									
Saint Vincent basalt (glass), starting and recovered samples from XRD experiments										
PC82**	46.91	1.37	15.16	0.95	11.58	10.58	2.98	0.50	2.97	96.59
3.5 GPa-1600 °C	(0.51)	(0.27)	(0.09)	(0.15)	(0.18)	(0.08)	(0.58)	(0.04)	(0.22)	
PC83	47.95	1.36	15.57	1.24	12.33	10.94	2.84	0.46	2.90	95.59
3.5 GPa-1600 °C	(0.92)	(0.10)	(0.47)	(0.13)	(0.19)	(0.34)	(0.18)	(0.07)	(0.14)	(1.28)
APS run 13	47.16	1.30	15.42	0.70	12.42	10.78	2.55	0.38	2.26	93.2
4.7 GPa-1600 °C	(0.86)	(0.07)	(0.40)	(0.10)	(0.23)	(0.18)	(0.11)	(0.09)	(0.19)	(1.13)
APS run 26	51.14	1.14	16.52	0.58	12.97	11.57	2.41	0.48	–	97.06
4.9 GPa-1600 °C	(0.93)	(0.11)	(0.32)	(0.15)	(0.16)	(0.27)	(0.11)	(0.05)	–	(0.72)
Etna basalt (glass), recovered samples from XRD experiments										
APS Etna2002	49.38	1.92	18.35	3.86	5.91	11.38	3.63	2.24	–	96.91
1.0 GPa-1250 °C	(0.46)	(0.15)	(0.40)	(0.37)	(0.14)	(0.25)	(0.16)	(0.24)	–	(0.79)
APS 20BaM19	46.79	1.94	17.31	3.88	6.88	11.49	3.82	2.06	0.80	95.20
1.3 GPa-1120 °C	(0.66)	(0.10)	(0.29)	(0.04)	(0.10)	(0.31)	(0.13)	(0.13)	(0.09)	(0.81)
Etna basalt (glass+clinopyroxenes), recovered samples from X-ray diffraction (XRD) experiments										
APS TGH25 glass	49.73	2.00	19.20	7.04	3.55	8.40	4.73	2.91	–	97.85
3.7 GPa-1450 °C	(0.97)	(0.05)	(0.28)	(0.34)	(0.09)	(0.32)	(0.17)	(0.21)		(1.19)
APS TGH27 glass	50.30	1.85	19.31	3.52	4.35	7.55	4.76	3.09	1.15	96.23
3 GPa-1550 °C	(0.58)	(0.11)	(0.54)	(0.23)	(0.16)	(0.17)	(0.21)	(0.19)	(0.10)	(0.17)

* Note that ‘Total’ does not include water content, that varies from 1.6(0.3) to 3.8(0.5) wt% as measured only for PC83 and PC82 respectively Leroy *et al.* [2019].

** Data from Leroy *et al.* [2019]. Note that Etna basalt samples were recovered from XRD experiments still embedded in their diamond capsule, hence high quality polishing could not be achieved.

metallic iron (Figure 2c), indicating reduction from FeO. This is not observed in recovered Saint Vincent glasses, as those contained very little FeO in the starting glass (less than 1 wt%, Table 1), and remained homogeneous (Figure 2b).

3.2. Melt structure: X-ray diffraction

To investigate the effect of iodine on melt structure, both I-doped and I-free basaltic melts were probed. In case of co-existence of melt and crystals, the press was moved relative to X-ray beam position until area free of crystals could be probed. Amongst the three pairs of I-doped/I-free runs (Table 1), two provided sufficiently high quality data to extract radial

distribution functions (APS runs 13/26 and APS TGH25/27, Figure 3). The structure factor, $S(q)$, of the I-doped melts have a weaker first-sharp diffraction peak (highest intensity near 2 \AA^{-1} on Figure 3 left panel) compared to the I-free melts, indicative of a lesser degree of medium-range order [Salmon, 1994], in other words, a lesser degree of polymerisation. APS runs 13 and 26 have different hydration levels in the starting samples (1.6 vs 3.8 wt% H₂O), which also contributes to a lesser degree of depolymerisation in I-doped APS run 13. However Etna basalts were not hydrated prior to XRD experiments, but are similarly impacted by the presence of iodine.

The effect of iodine on the radial distribution function $g(r)$ (Figure 3 right panel) is less

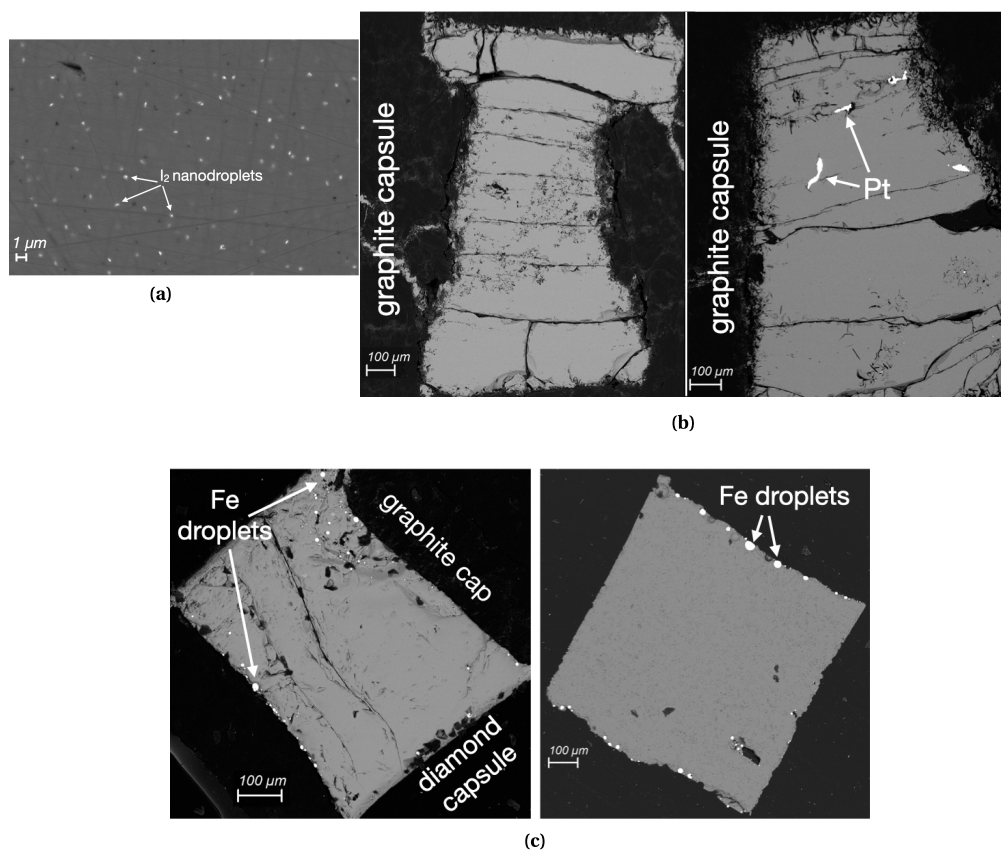


Figure 2. SEM images of quenched glasses recovered from piston-cylinder runs and in situ high P - T X-ray diffraction (XRD) experiments. (a) Starting sample PC82 (Saint Vincent basalt, I-doped). (b) Saint Vincent basalt in graphite capsule recovered from XRD experiments (left: run 13, I-doped, right: run 26, I-free). (c) Etna basalt recovered from XRD experiments (left: 20BaM19, I-doped, in diamond capsule, right: Etna2002, I-free, extracted from diamond capsule). Bright zones are either I_2 droplets (a), Pt bits inherited from the previous piston-cylinder run using Pt capsules (b right), or metallic Fe droplets (c).

pronounced. The small contribution near 3 \AA^{-1} on $S(q)$ for run APS TGH27 stems from dispersed Fe droplets in the magma, and translates into a contribution peaking at 2.5 \AA^{-1} on $g(r)$, consistently with reported XRD data on molten Fe [Sanloup *et al.*, 2000] and with the observation of Fe droplets on recovered samples (Figure 2c). Interestingly, we do not observe this contribution of molten Fe for the I-free run APS TGH25, attesting that reduction of Fe was less extensive in the I-free basalt (Table 1). Diffusion of hydrogen through the Pt-Rd caps, and/or diffusion of C from the inner graphite caps, can not be excluded as other causes of Fe reduction, but the difference between I-free and I-doped samples is significant.

To better evidence the contribution of iodine atoms to the radial distribution function, we used the APS run13/26 datasets, that are not impacted by the contribution of molten Fe to the XRD signal. The difference between reduced radial distribution functions, $G(r) = 4\pi r\rho(g(r) - 1)$, for I-doped and I-free basalts was calculated after normalisation of $g(r)$ to the Si-O contribution (Figure 4). Note that while this procedure enables to evidence interatomic distances, it is not sufficient to calculate accurate coordination numbers. To do so, the full $g(r)$ should be simulated against the sum of all partial pair distribution functions, but this is challenging for such small differences. Two interatomic distances

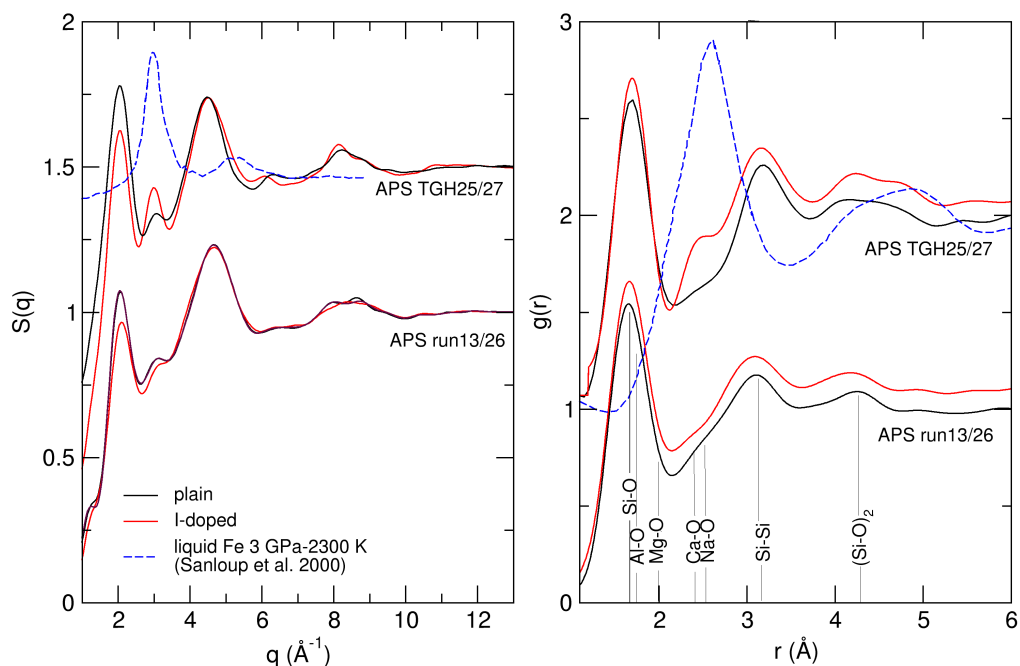


Figure 3. Right panel: structure factors, $S(q)$; left panel: radial distribution functions, $g(r)$.

are visible at 2.2 \AA and at 3.5 \AA (Figure 4), and due to the normalisation procedure to the Si-O contribution, we cannot exclude that distances shorter than 2 \AA also exist. These contributions are either I-related or enhanced contributions due to the presence of iodine. XRD is sensitive to the electrons, the intensity of the signal evolves with Z^2 (Z , atomic number). Iodine being a very heavy element, its scattering is 4 times stronger than that of Fe, and 14 times stronger than that of Si. Hence the likeliest possibility is that differences on radial distribution function between I-doped and I-free basalts are due to iodine, and not to other elements even if their abundances may vary slightly. The potential contribution of Fe-O nevertheless needs to be discussed, as its contribution to $g(r)$ in a basalt is at 2.07 \AA and 3.4 \AA (Fe-O and Fe-Fe interatomic distances respectively [Guillot and Sator, 2007]), all other main interatomic distances being different (see position of main cation-oxygen interatomic distances on Figure 3). However, it cannot be the case since FeO content is similar between I-free and I-doped Saint Vincent basalt, and this content is lower than 1 wt% hence the expected contribution is very low. These

additional contributions in I-doped $G(r)$ can neither be attributed to an eventual P difference between I-doped and I-free basalts. The maximum P (4.9 GPa) reached in these experiments can induce changes of coordination number for some cation-oxygen bonds, but it is way too modest to induce a contraction of interatomic distances. Na-O for instance contracts by 0.02% between 0 GPa and 5 GPa [Karki et al., 2018], all other main cation-oxygen distances change even less.

Amongst reported I-X bonds for iodine compounds, the 2.2 \AA distance is shorter than iodine-iodine (2.7 \AA) or iodine-metal bonds (3.2 \AA -4.0 \AA), and closer to iodine-oxygen bonds reported for crystalline iodates (1.8-2.2 \AA range), the longest I-O bonds corresponding to medium intramolecular bonds with a single covalent bond character [Gautier-Luneau et al., 2010, Abudouwufu et al., 2020], indicative that we are not looking at IO_3^- units here (I-O bond length nearer 1.8 \AA), but at more complex iodates. The longer 3.5 \AA distance is too long for Na-I or Ca-I, but matches well with the I-I interatomic distance in polyiodates such as $\text{K}_2\text{Na}(\text{IO}_3)_2(\text{I}_3\text{O}_8)$ [Abudouwufu et al., 2020].

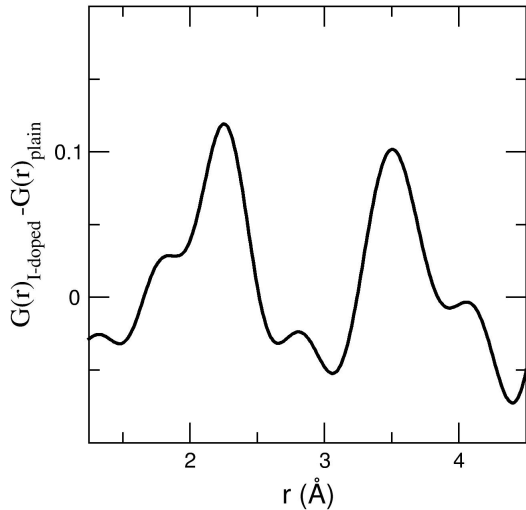


Figure 4. The iodine contribution to the reduced $G(r)$ radial distribution function, as obtained from the difference between APS run 13 and APS run 26 XRD datasets.

3.3. Melt structure: Raman spectroscopy

Some starting and recovered samples were analysed by Raman spectroscopy (Figure 5). We note that it is difficult to obtain Raman spectra on these natural compositions due to an inherent high level of fluorescence, and in particular in the intramolecular water range (e.g. [2800–3600] cm^{-1}). Iodine–iodine signature is visible on starting sample PC82, with bands at 114 cm^{-1} and 154 cm^{-1} , consistently with the observation of nano-size iodine (I_2) bubbles by SEM (Figure 2a), bands that are also observed in the I-richest borosilicate glass in Cicconi *et al.* [2019] and were attributed to NaI bonds but seem more consistent with I_2 signal. There is no visible iodine–iodine nor metal–iodine contribution on any spectra measured on samples recovered from XRD experiments. Instead there is the systematic presence of four small but clear vibrational bands in I-doped samples at 615 cm^{-1} , 647 cm^{-1} (this one on top of a broader band by comparison with I-free samples), 1098 cm^{-1} , and 1177 cm^{-1} . Interestingly, there is also a broad band circa 640–660 cm^{-1} in I-doped borosilicate glasses (Figure 5), albeit not discussed by the authors. While we are most likely observing oxidized iodine in these glasses, it is not in the form of IO_3^- units that give rise to bands in the [700–800] cm^{-1}

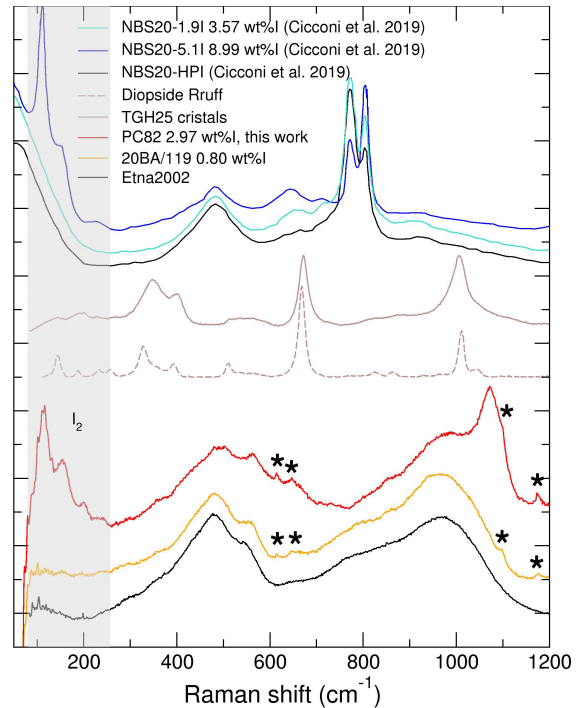


Figure 5. Raman spectra collected on an iodine over-saturated sample (PC82), and on two recovered samples from in situ X-ray diffraction experiments (I-doped 20BA/M19 and I-free Etna2002), Raman spectra collected on I-doped and plain borosilicate glasses (NBS20) [Cicconi *et al.*, 2019] are shown for comparison. For I-doped basaltic glasses, I_2 related modes are observed below 200 cm^{-1} for PC82 (grey shaded area), and iodate-related modes are marked by asterisks. Note that PC82-Saint Vincent basaltic composition (3.8 wt% H_2O) is less polymerised, as seen by the increased band near 1070 cm^{-1} . For borosilicate glasses, the strong bands in the [740–840] cm^{-1} are related to borate rings and boroxol.

range [Cicconi *et al.*, 2019], but of more complex iodate forms alike hydrated periodate groups. For instance, mixed salt $\text{Cs}_2[\text{I}(\text{OH})_3\text{O}_3]\cdot\text{CsSO}_4(\text{H})\text{H}_5\text{IO}_6$ has its strongest band at 651 cm^{-1} , attributed to I-O IO_6^- symmetric stretching vibration [Romanchenko *et al.*, 2004]. The two highest Raman shift modes fall within the range reported for δ I–O–H modes in octahedral periodates, i.e. [1050–1190] cm^{-1} [Dengel *et al.*, 1993].

4. Discussion

Iodine induces changes in the silicate melt network structure, observed here by a lesser degree of polymerisation as probed by X-ray diffraction, and reported on the basis of Raman spectroscopy on Fe-free alkali-rich felsic magmas [Faranda, 2023], and Fe-free borosilicate glasses [Cicconi et al., 2019, Morizet et al., 2021]. While this behaviour is noticeable for experimental levels of I-doping in the order of 1 or more wt%, and is a relevant property in the context of nuclear waste glasses, it is not expected for natural levels of I content in magmas. The network modifying role of I however does indicate that I is not retained passively in the voids or in the ring structure of magmas, nor that it removes Na or K ions from the melt oxides otherwise the opposite effect would be observed, i.e. enhanced polymerisation.

The coexistence of reduced iodide (I^-) and oxidized iodate (IO_3^-) species in SiO_2 poor (14–33 wt% SiO_2) borosilicate glasses [Cicconi et al., 2019] synthesized at 1.5 kbar in the B_2O_3 – SiO_2 – Na_2O system, was reported based on combined Raman and X-ray Absorption Near Edge Structure (XANES) spectroscopies. However, as mentioned above, the Raman data also showed vibrational modes corresponding to IO_6^{5-} groups. More complex high P aluminoborosilicate glasses in the system SiO_2 – Al_2O_3 – B_2O_3 – CaO – Na_2O investigated by X-ray photoelectron and extended X-ray absorption spectroscopies have a large predominance of iodide species [Morizet et al., 2021], in addition to iodates for their most SiO_2 poor composition (NH glass, 43 wt% SiO_2), although reconciling information from both types of spectroscopies proved difficult. It is important to note that borosilicate glasses are not ideal analogues for basaltic melts, but they share the same characteristic to have a low degree of polymerisation and high I solubility. Last but not least, Leroy et al. [2019] observed only I_2 signals on in situ Raman spectra of I-doped haplogranite melt coexisting with hydrous fluid. This points out that I speciation depends on magma polymerisation, e.g. on the $SiO_2+Al_2O_3$ content, and also on its FeO content. This, in turn, could underpin the lower solubility of I in SiO_2 -rich well polymerised magmas [Cicconi et al., 2019, Leroy et al., 2019].

The potential role of FeO is highlighted here by the amount of reduced iron that is higher for I-doped

samples than I-free samples run for similar duration at high T (TGH25 and TGH26, Table 1), indicating that FeO was the likely source of oxygen to form periodates, leading to the formation of metallic Fe. This effect is unfortunately not clear for I-free Etna2002 compared to I-doped 20BA/M19, with similar FeO content in the quenched glass which could result from Etna2002 shorter run duration. In the case of Saint Vincent basalt experiments, the starting glass was already almost FeO free (Table 1) after piston-cylinder press iodine and water doping using platinum capsules. Hence the most obvious source of oxygen was water for this composition.

Iodine speciation in basalts as an oxide is quite unique amongst halogens elements. X-ray absorption spectroscopy measurements on glasses recovered from high P – T conditions have mostly targeted chlorine and bromine speciation so far. Chlorine bonds to network modifying cations [Evans et al., 2008, Thomas et al., 2023], in particular to Ca, Fe and Mg, to a lesser extent to Na, and in the case of the most SiO_2 rich melts also to Si [Thomas et al., 2023]. The higher affinity of chlorine for alkaline-earth cations than for alkaline cations was confirmed for borosilicate glasses [Jolivet et al., 2023]. Bromine speciation in silica-rich magmas changes between low P , with Br–Na bonds and a hydration shell, to a closer oxygen environment above 2 GPa [Cochain et al., 2015, Louvel et al., 2020] although whether oxygen belongs to water molecules or to the silicate network could not be deciphered. Bromine speciation besides remains to be investigated in basaltic compositions. The bulk silicate Earth (BSE) contains approximately ten times more Br than I [Kendrick et al., 2017, Guo and Korenaga, 2021], the Br/I ratio raises in MORB and arc basalts (circa 50, [Kendrick et al., 2014]), and even slightly more in atmospheric volcanic plumes (58–87, [Aiuppa et al., 2005]). Differences in Br and I speciation in magmas could, at least partially, underpin this behaviour.

5. Conclusion

While iodine is generally thought as present in nature either as iodide (I^-), iodate (IO_3^-), or elemental iodine (I_2), we show here that it is stable in basaltic melts and glasses as a more complex iodate such as polyiodates or orthoperiodates. It is thus possible that this peculiar speciation of iodine might have been

missed in past investigations, in particular when using spectroscopic methods that require the collection of data on reference materials and for which only I^- , I_2 and IO_3^- were looked for. An alternative to reference materials is to use an input model, but this is very difficult to have for non-crystalline materials. In this respect, the X-ray diffraction method used here is not standard- nor model-dependent. But it can only be applied to the study of the heaviest—hence most scattering—I element. Indeed, with solubilities reaching only a few wt% in compressed basalts, its detection is clear but remains small, demonstrating that any lighter halogen element will not be detectable by this method. Iodine as orthoperiodate is observed in basaltic melts generated between 1.5 GPa and 4.9 GPa in the present study, but similarity in Raman spectroscopy data shows that this oxidized state extends to SiO_2 -poor borosilicate melts at 1.5 kbar [Cicconi *et al.*, 2019]. It does not however extend to SiO_2 -rich compositions, as only I_2 signal was observed on Raman spectra measured on compressed I-doped haplogranite melt [Leroy *et al.*, 2019], and mostly as iodide in SiO_2 -rich high P aluminoborosilicate glasses [Morizet *et al.*, 2021].

Interestingly, formation of iodates has also been observed during circulation of water-iodide solutions through volcanic rock cores at ambient conditions [Neil *et al.*, 2020], on the basis of UV spectroscopy measurements. This was interpreted as resulting from the retention of oxidized I by minerals in volcanic rocks, concomitantly with reduction of ferric ions. In conjunction with the present results, this points out that future studies should be dedicated to elucidating simultaneously the speciation of I and Fe in magmas to fully understand I behaviour in petrologic and volcanic processes.

Declaration of interests

The authors do not work for, advise, own shares in, or receive funds from any organization that could benefit from this article, and have declared no affiliations other than their research organizations.

Acknowledgments

Natural basaltic samples from Saint Vincent and Mount Etna were provided by G. Prouteau from Institut des Sciences de la Terre d'Orléans. We acknowledge K. Curtis-Benson for providing parts for

cell assemblies and arranging shipments before and after experiments at the Advanced Photon Source, K. Béneut for use of the Raman spectroscopy platform at IMPMC, O. Boudouma for SEM measurement and N. Rivodini for EPMA analyses at OSU Ecce Terra, Sorbonne Université. This work was supported by the European Research Council under the European Community's Seventh Framework Programme (FP7/20072013 Grant Agreement No. 259649 to CS), TG was supported by the ANR Projet de Recherche Collaborative VOLC-HAL-CLIM (Volcanic Halogens: from Deep Earth to Atmospheric Impacts, ANR-18-CE01-0018) and is grateful for an EU Marie Skłodowska-Curie Fellowship "ExCliso" (Project ID 101017762), QC was supported by CSC scholarship (#201806340094). HPCAT operations are supported by DOE NNSA's Office of Experimental Sciences. The Advanced Photon Source is a U.S. Department of Energy (DOE) Office of Science User Facility operated for the DOE Office of Science by Argonne National Laboratory under Contract No. DE-AC02-06CH11357.

References

- Abudouwufu, T., Zhang, M., Cheng, S., Zeng, H., Yang, Z., and Pan, S. (2020). $K_2 Na(IO_3)_2 (I_3O_8)$ with strong second harmonic generation response activated by two types of isolated iodate anions. *Chem. Mater.*, 32(8), 3608–3614.
- Aiuppa, A., Federico, C., Franco, A., *et al.* (2005). Emission of bromine and iodine from Mount Etna volcano. *Geochem. Geophys. Geosystems*, 6, article no. Q08008.
- Bureau, H., Keppler, H., and Métrich, N. (2000). Volcanic degassing of bromine and iodine: experimental fluid/melt partitioning data and applications to stratospheric chemistry. *Earth Plan. Sci. Lett.*, 183(1–2), 51–60.
- Cicconi, M. R., Pili, E., Grousset, L., Florian, P., Bouillard, J. C., Vantelon, D., and Neuville, D. R. (2019). Iodine solubility and speciation in glasses. *Sci. Rep.*, 9, article no. 7758.
- Cochain, B., Sanloup, C., de Grouchy, C., Crépinsson, C., Bureaud, H., Leroy, C., Kantor, I., and Irifune, T. (2015). Bromine speciation in hydrous silicate melts at high pressure. *Chem. Geol.*, 404, 18–26.
- Cuevas, C. A., Fernandez, R. P., Kinnison, D. E., *et al.* (2022). The influence of iodine on the Antarctic

- stratospheric ozone hole. *Proc. Natl. Acad. Sci. USA*, 119(7), article no. e2110864119.
- Dengel, A., Griffith, W., Mostafa, S., and White, A. (1993). Raman and infrared study of some metal periodato complexes. *Spectrochim. Acta A*, 49(11), 1583–1589.
- Evans, K. A., Mavrogenes, J. A., O'Neill, H. S., Keller, N. S., and Jang, L. Y. (2008). A preliminary investigation of chlorine XANES in silicate glasses. *Geochem. Geophys. Geosystems*, 9, article no. Q10003.
- Faranda, F. (2023). *Behavior of halogens (Cl, Br, I) in alkali-rich felsic magmas at crustal depth : an experimental approach*. Phd thesis, Université d'Orléans, France.
- Gautier-Luneau, I., Suffren, Y., Jamet, H., and Pilme, J. (2010). Reinterpretation of three crystal structures of alkali oxiodate(v) - description of the $[I_3O_8]^-$ anion and the infinite 2D $[I_3O_8]_{\infty}^-$ anion. *Z. Anorg. Allg. Chem.*, 636(7), 1368–1379.
- Gennaro, E., Iacono-Marziano, G., Paonita, A., Rottolo, S. G., Martel, C., Rizzo, A. L., Pichavant, M., and Liotta, M. (2019). Melt inclusions track melt evolution and degassing of Etnean magmas in the last 15 ka. *Lithos*, 324, 716–732.
- Guillot, B. and Sator, N. (2007). A computer simulation study of natural silicate melts. Part I: low pressure properties. *Geochim. Cosmochim. Acta*, 71, 1249–1265.
- Guo, M. and Korenaga, J. (2021). A halogen budget of the bulk silicate Earth points to a history of early halogen degassing followed by net re-gassing. *Proc. Natl. Acad. Sci. USA*, 118(51), article no. e2116083118.
- Jolivet, V., Morizet, Y., Trcera, N., Fernandez, V., and Suzuki-Muresan, T. (2023). Incorporation of chlorine in nuclear waste glasses using high-pressure vitrification: Solubility, speciation, and local environment of chlorine. *Am. Mineral.*, 108(6), 1032–1042.
- Karki, B. B., Ghosh, D. B., and Bajgain, S. K. (2018). *Simulation of Silicate Melts Under Pressure*. Elsevier, Amsterdam. chapter 16.
- Kendrick, M. A., Arculus, R. J., Danyushevsky, L. V., Kamenetsky, V. S., Woodhead, J. D., and Honda, M. (2014). Subduction-related halogens (Cl, Br and I) and H₂O in magmatic glasses from Southwest Pacific Backarc basins. *Earth Plan. Sci. Lett.*, 400, 165–176.
- Kendrick, M. A., Hemond, C., Kamenetsky, V. S., Danyushevsky, L., Devey, C. W., Rodemann, T., Jackson, M. G., and Perfit, M. R. (2017). Seawater cycled throughout Earth's mantle in partially serpentinized lithosphere. *Nat. Geosci.*, 10(3), 222–228.
- Kendrick, M. A., Woodhead, J. D., and Kamenetsky, V. S. (2012). Tracking halogens through the subduction cycle. *Geology*, 40(12), 1075–1078.
- Kono, Y., Irifune, T., Higo, Y., Inoue, T., and Barnhoorn, A. (2010). P–V–T relation of MgO derived by simultaneous elastic wave velocity and in situ x-ray measurements: A new pressure scale for the mantle transition region. *Phys. Earth Planet. Int.*, 183, 196–211.
- Kono, Y., Park, C., Kenney-Benson, C., Shen, G., and Wang, Y. (2014). Toward comprehensive studies of liquids at high pressures and high temperatures: Combined structure, elastic wave velocity, and viscosity measurements in the Paris-Edinburgh cell. *Phys. Earth Planet. Int.*, 228, 269–280.
- Leroy, C., Bureau, H., Sanloup, C., et al. (2019). Xenon and iodine behaviour in magmas. *Earth Planet. Sci. Lett.*, 522, 144–154.
- Louvel, M., Sanchez-Valle, C., Malfait, W. J., Pokrovski, G. S., Borca, C. N., and Grolimund, D. (2020). Bromine speciation and partitioning in slab-derived aqueous fluids and silicate melts and implications for halogen transfer in subduction zones. *Solid Earth*, 11(4), 1145–1161.
- Morizet, Y., Jolivet, V., Trcera, N., Suzuki-Muresan, T., and Hamon, J. (2021). Iodine local environment in high pressure borosilicate glasses: An x-ray photoelectron spectroscopy and x-ray absorption spectroscopy investigation. *J. Nucl. Mater.*, 553, article no. 153050.
- Muramatsu, Y. and Wedepohl, K. (1998). The distribution of iodine in the Earth's crust. *Chem. Geol.*, 147(3–4), 201–216.
- Neil, C. W., Telfeyan, K., Sauer, K. B., Ware, S. D., Reimus, P., Boukhalfa, H., Roback, R., and Brug, W. P. (2020). Iodine effective diffusion coefficients through volcanic rock: Influence of iodine speciation and rock geochemistry. *J. Contam. Hydrol.*, 235, article no. 103714.
- Pichavant, M., Mysen, B. O., and Macdonald, R. (2002). Source and H₂O content of high-MgO magmas in island arc settings: an experimental study of a primitive calc-alkaline basalt from St. Vincent,

- Lesser Antilles arc. *Geochim. Cosmochim. Acta*, 66, 2193–2209.
- Romanchenko, E., Shilov, G., Dobrovolskii, Y., Chernyak, A., Karelin, A., and Atovmyan, L. (2004). Mixed salt $\text{Cs}_2[\text{I}(\text{OH})_3\text{O}_3] \cdot \text{CsSO}_4(\text{H})\text{H}_5\text{IO}_6$: Synthesis, crystal structure, and properties. *Russ. J. Coord. Chem.*, 30(7), 453–458.
- Salmon, P. S. (1994). Real space manifestation of the first sharp diffraction peak in the structure factor of liquid and glassy materials. *Proc. Math. Phys. Sci.*, 445, 351–365.
- Sanloup, C., Guyot, F., Gillet, P., Fiquet, G., Hemley, R., Mezouar, M., and Martinez, I. (2000). Structural changes in liquid Fe at high pressures and high temperatures from synchrotron x-ray diffraction. *Europhys. Lett.*, 52, 151–157.
- Solomon, S., Garcia, R., and Ravishankara, A. (1994). On the role of iodine in ozone depletion. *J. Geophys. Res. Atmos.*, 99(D10), 20491–20499.
- Thomas, R. W., Wade, J., and Wood, B. J. (2023). The bonding environment of chlorine in silicate melts. *Chem. Geol.*, 617, article no. 121269.
- Webster, J. D., Baker, D. R., and Aiuppa, A. (2018). Halogens in mafic and intermediate-silica content magmas. In Harlov, D. and Aranovich, L., editors, *Role of Halogens in Terrestrial and Extraterrestrial Geochemical Processes: Surface, Crust, and Mantle*, pages 307–430. Springer Geochemistry, Cham.
- Yamada, A., Wang, Y., Inoue, T., Yang, W., Park, C., Yu, T., and Shen, G. (2011). High-pressure x-ray diffraction studies on the structure of liquid silicate using a Paris-Edinburgh type large volume press. *Rev. Sci. Instrum.*, 82, article no. 015103.